In: Wireless Communications Research Trends
Editor: Tong S. Lee, pp. 223-260
ISSN: 978-1-60021-674-9
© 2007 Nova Science Publishers, Inc.

Chapter 7

MEMS MICRO-ANTENNAS FOR WIRELESS BIOMEDICAL SYSTEMS

P.M. Mendes and J.H. Correia
Department of Industrial Electronics, University of Minho
Campus de Azurém, 4800-058 Guimarães, Portugal

Abstract

Invasive and implantable biomedical devices used for diagnostic and therapy, ranging from neural prosthesis to video-capsule endoscopy (VCE) systems, are emerging innovative technologies and they are expected to originate significant business activity in the near future. The success of such systems is in part due to the advent of microtechnologies, which made possible the miniaturization of several sensors and actuators, as well their integration with readout and communication electronics.

The new biomedical devices offer the possibility of improved quality of life, as well cost savings associated with health care services. However, one open challenging is to communicate to and from a biomedical device placed inside the human body with devices outside the human body. The lack of antennas, small enough to be integrated with the sensing microsystem, is a difficult task to overcome because such communications must be made at relatively low frequencies, due to live tissue signal attenuation. The straightforward solution is to increase the devices size to dimensions where it becomes possible to integrate an antenna. Up to now solutions, use conventional antennas together with miniaturization techniques to achieve the smallest antennas possible. However, the size of such devices is usually limited by the antenna and, is some cases, also by the batteries size.

Micro-Electro-Mechanical Systems (MEMS) are becoming an available option for RF communication systems since they can offer, simultaneously, devices with improved performance and they use IC-compatible materials, allowing their integration in a silicon chip, side by side with semiconductor circuits. Up to now, MEMS have been used for antenna applications to obtain non-conventional front-ends with improved, or new characteristics. However, some preliminary tests have shown that some MEMS structures could have the ability to operate as an antenna itself and this solution would have the potential to be smaller than the conventional antennas.

In this chapter, it is first discussed the need for small wireless biomedical devices. This requires the use of a microsystem completely integrated, from sensors to communications, thus requiring the use of integrated antennas. The electrical properties of substrates available

in integrated circuit technology are very important for antenna design and one method used to characterize wafer materials is presented. Moreover, the antenna integration requires the availability of an electrically small antenna fabricated on materials compatible with the fabrication of integrated circuits. This integration requires the use MEMS techniques, like micromachining and wafer level packaging.

Finally, MEMS structures previously used for non-conventional front-ends will be introduced and investigated, having in mind a new application, the MEMS structure itself will be operating as an antenna. The development of new integrated antennas using MEMS solutions has the potential to make the devices smaller and more reliable, which will make them cheaper and adequate for mass production, resulting in a key advantage for competitors in the RF market. Also, the availability of smaller biomedical wireless devices can lead to new applications not yet fully envisioned. The new solutions envisions power saving, smaller volume, lower cost, and increased system lifetime, which are very important features in biomedical microsystems for diagnosis and therapy.

Wireless Biomedical Devices

Introduction

Sensor networks are expected to be the 21st century holly Graal in sensing. Wireless sensor networks are an emerging technology that brings not only numerous opportunities but also many technological challenges. Ranging from automotive to home applications, sensor are expected to become part of our daily live. There are various physical quantities in different environments that, when measured and recorded, could bring new quality to our lives. If, e.g., soil properties like humidity, temperature, chemical composition, could be measured in a distributed way, providing detailed local data for an entire farm field, the watering and nutrition supply could be adapted locally resulting in optimum growing conditions and thus significant environmental savings.

To be effective and to have the ability to adapt itself to complex environments, like a farm field, an office building, or a human body, each sensor node has to be autonomous. This means that, desirably, it should be self-powered and provided with wireless communications. This type of systems usually requires low power consumption (battery life-time) and uses low data-rate communications (small bandwidth), requiring special design. The wireless sensor networks technology is also moving to biomedical applications. Due to the high number of microsensors and microactuators, the monitorization of several physiological parameters is now available. Moreover, application of distributed sensing systems will highly be facilitated if cheap and easy-to-use ‘on-chip’ or ‘in-package’ solutions, equipped with short-range wireless communication capabilities, would be available.

With a widespread and increased sophistication of medical implants, new solutions will be required for flexible and small modules to communicate with the implant. Today’s most common solution is to use an inductive link between the implant and an external coil. The main drawback of this solution is the small range achieved (not more than a few centimetres). However, this link can be used also to power the implanted device.

Application of wafer-level chip-scale packaging (WLCSP) techniques like adhesive wafer bonding and through-wafer electrical via formation, combined with the selected radio frequency (RF) structures allows a new level of antenna integration. However, these new techniques require the combination of new materials with the standard materials used for

integrated circuits fabrication. In this way, together with substrate processability, the knowledge of accurate electrical parameters is of extreme importance when designing for RF or microwave applications.

Applications

The traditional endoscopic techniques shows limitations in their range for the different segments of the digestive tract, namely in the small intestine. Through the gastroscopy, it is possible to access the gastrointestinal proximal tract (gullet, stomach, and duodenum). In the other hand, through colonoscopy the access is almost limited to the colon, leaving inaccessible some parts of the small intestine. When a patient suffers from bleeding in the gastrointestinal tract and the endoscopy doesn't answer the diagnostic needs, it is necessary to use the traditional radiographic or cintilographic techniques. However, with these techniques is very hard to detect bleeding sources in the small intestine [1]. Moreover, the endoscopic diagnostic is a very uncomfortable procedure for the patients and requires highly skilled medical doctors.

One possible solution to overcome those limitations is to use an innovative technique known by video capsule endoscopy, also known by smart pill, capsule camera, or wireless capsule camera. The patient swallows the endoscopic capsule and it takes photos from the different places during its travel through all the digestive tube. In this way, it is possible to obtain access, even in a limited way, to areas in the small intestine previously accessible only by surgical and invasive procedures [2]. The camera-in-a-pill is a very promising technique since after its availability the approx. 5 meters of the small intestine become accessible [3]. Since its development in the eighties, the endoscopic capsule is changing the way we deal with the diseases in the small intestine, and its use is now being extended to the gullet [4].

The endoscopic capsule is neither provided with locomotion nor with stop mechanism, making its way due to peristaltic movements. The control of the capsule locomotion would allow new procedures like biopsies (detection of tumours) or drug delivery, and is an ongoing research topic. Together with locomotion, before we can fully benefit from this technology, miniaturized modules are required to implement the wireless communications to and from the capsule with devices outside the human body.

This is an open challenge, not only for VCE, but also for all the biomedical devices that are implanted inside the human body, like FES systems [5]. As an application example, several people from all ages suffer from incontinence or other urinary pathologies. The bladder and the intestines perform their function in an autonomous way, independently from the voluntary control. However, any disorder in the healthy behaviour leads to the problem of urinary incontinence, bladder infections, low bladder capability and faecal incontinency. The International Continence Society (ICS) defines incontinence as the involuntary loss of bladder or bowel control. Urinary incontinence (UI) is a stigmatised, underreported, under-diagnosed, under-treated condition that is erroneously thought to be a normal part of aging. One-third of men and women ages 30-70 believe that incontinence is a part of aging to accept [6]. The social costs of UI are high and even mild symptoms affect social, sexual, interpersonal, and professional function [7].

The healthy working of the urinary tract is essential for health and well-being in general, and even more critical for patients with lesions in the spinal cord. In this situation, catheters

are commonly used to control the daily volume of urine inside the bladder. However, the complications related to the use of catheters, together with the fact that, most of the times, the spinal segments which controls the bladder are intact, are driving the development of several devices to improve the control the inferior urinary system [8].

From the anatomy of the spinal cord, the microsystem could be designed to operate, or in the epidural space, or in the subarachnoid space, allowing the duramater to be completely closed after surgical intervention. The available subarachnoid space varies between 3 mm and 9 mm [9]. This is room enough to accommodate a small microdevice, but the antenna may become a problem.

Other field becoming very popular, where the nanotechnologies are giving a contribution, is related with neural signal recording and stimulation. The accurate record of neural signal requires the use of very small wireless bio-devices for invasive biopotential monitoring [10].

The full system integration is difficult to achieve because the communications must, preferably, be made at low frequencies, due to live tissue signal attenuation, and there is a lack of antennas small enough to be integrated with the sensing microsystem. The adopted solution is to increase the devices size to dimensions where it becomes possible to integrate an antenna. Up to now solutions, use conventional antennas together with miniaturization techniques to achieve the smallest antennas possible [11, 12]. However, the size of such devices is usually limited by the antenna and, is some cases, also by the batteries size.

System Requirements

Frequency and Bandwidth

A wireless microsystem uses the surrounding environment as the communicating channel. This channel is available in different spectral regions, which corresponds to a different channel frequency, bandwidth, and attenuation. For biomedical applications, the surrounding environment is the human body, a highly heterogeneous environment.

In this environment, the attenuation may become highly severe when the antenna miniaturization is required because a smaller antenna is commonly obtained with an increase in the operating frequency. Fig. 1 shows the signal attenuation for a tissue with a high content of water [13]. The figure shows the penetration depth, i.e., the depth where the power density is 13.5 % below the incident power density.

This figure must be used carefully and only as an indication for attenuation since it can be very different for different water concentration in the tissue. However, it can be observed an increase in the attenuation for higher frequencies. This means that the biomedical devices should use low frequencies if low power is required for communications. Despite all freedom of choice about the frequencies that should be used, there is an adoption of ISM (*Industrial, Scientific and Medical*) bands. These bands plays a very important role in communications since they allow the development of wireless devices, where the constraints in terms of power level, frequency, and bandwidth are very well defined. The most common frequency bands we can find are in the 433 MHz range and in the 13 MHz range. These frequencies are very popular since they allow a good signal range in free-air and they are able to reach a few centimeters inside the human body. Moreover, the design of microdevices operating at such frequencies is a well-known process that requires low cost technology.

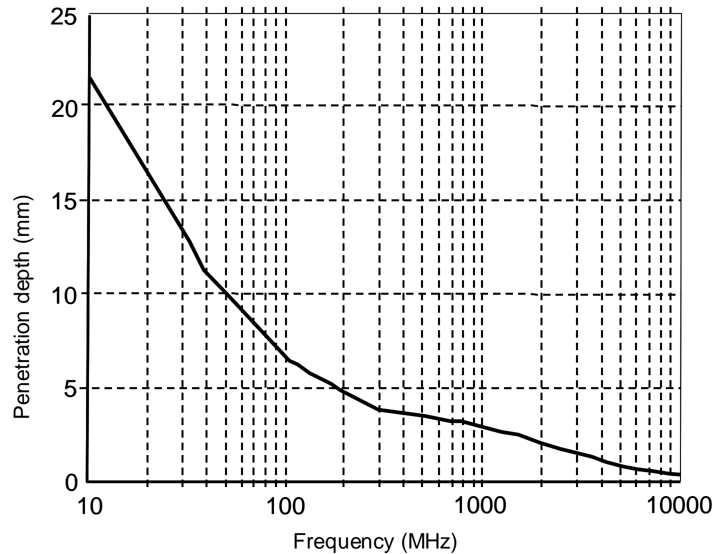

Figure 1. Penetration depth for a radio-frequency signal in a human body tissue.

Besides the radio-frequency communications, optical or ultrasonic communications are also very attractive options due to their possibilities for miniaturization. In optical communications, the main drawback are the high losses inside the human body and for ultrasonic the main drawback are the interfaces of the different tissues, which results in several reflections of the ultrasonic wave. Besides that, there is the interface air-human body that may kill the chance of a reliable communication. Notwithstanding all the drawbacks associated with signal attenuation and antenna integration, the radio frequency is one of the favourites for use in biomedical devices.

Despite all the deregulation that dominates the wireless communications for biomedical devices, except for the definition of ISM bands, the European Telecommunications Standards Institute (ETSI) has made an effort for standardization and specified the Medical Implant Communication System (MICS) [14]. The ETSI document applies to devices wiling to communicate between a base station and an implanted device and for devices wiling to communicate between medical implants within the same body.

The MICS uses the frequency band from 402 MHz to 405 MHz, with a maximum emission bandwidth of 300 kHz. Moreover, the maximum power limit is set to 25 μW Equivalent Radiated Power (ERP), i.e., the maximum field-strength in any direction should be equal to, or lower than, what a resonant dipole would give in its maximum direction at the same distance, with the dipole being fed with a signal of 25 μW.

Power

Like for frequency requirements, it’s very difficult to define what are power requirements for a biomedical device. Depending on the device power requirements, the power is provided either remotely or locally. Despite the MICS power level constrain, the power requirements for wireless biomedical devices are highly dependent on the target device. Some systems may have local power, using batteries or energy harvesting, and other systems require the use of remote power.

For devices that are power hungry, like functional electrical stimulating devices, the power, together with the required stimulus information, is provided by the wireless link. Depending on the use, a FES device for bladder control may require five 9 Volt batteries for one day of operation. On the other extreme are, e.g., hearing prosthesis, which use local power where power consumption must be below 1 mW. Also power hungry are the emerging VCE technology. These devices use local batteries since they are moving inside the human body and it is difficult to deliver power using the common solution with coils. In this system, the wireless link is only used for data transmission.

Antenna Design Options

From the previous sections it can be concluded that there is an emergent need for small biomedical devices fully integrated, antenna included. Moreover, the traditional coil does not provide a solution for systems requiring short-range communications [12]. This means that one must look for new solutions to integrate the antenna inside the biomedical microdevices.

Merging of antenna and circuitry leads to innovative RF front-end designs possessing several desirable features such as compactness, lower power consumption, and added design flexibility. Several approaches have been used to achieve antenna integration as summarized in Fig. 2. Antenna integration is a hard task to accomplish since it requires joining the knowledge from antennas, microwaves, circuit design, and materials. Moreover, the on-chip antenna integration requires an electrically small antenna, due to wafer cost and devices size constrains, and operating on a substrate that was not initially intended for that purpose.

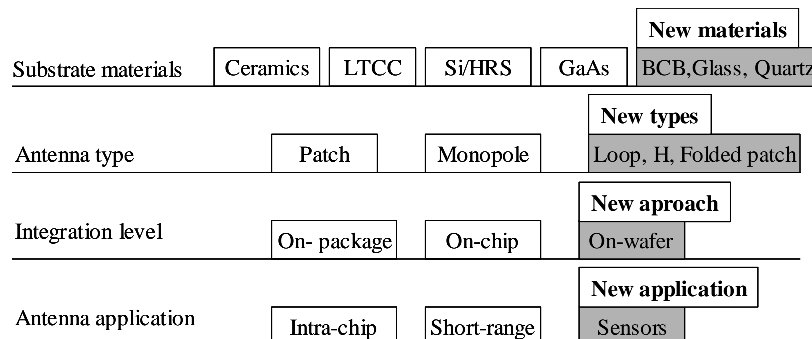

Figure 2. Summary of solutions for on-chip antenna integration.

Substrates

The antenna integration can be achieved with the direct placement of a radiator on the low-ohmic silicon. However, this approach requires a layer of thick oxide to reduce the losses or a proton implantation and still the obtained efficiencies are very low (~10 %).

Due to the high-losses observed on low-ohmic silicon, one way to improve the properties of integrated antennas may be to look for new materials with lower losses, but compatible with silicon processing. Up to now, several different materials have been used to implement on-chip antennas. GaAs has been used very often as antenna substrate due to its lower losses and high dielectric constant, which allows small and efficient antennas. However, since cost

and integrability is pushing RF circuitry to be implemented in CMOS, the use of high-resistivity silicon (HRS) was also been subject for several works. The use of HRS increases the antenna efficiency, keeps the antenna dimensions small, and allows easy integration with electronics. The main drawback is the increased wafers cost. On the other hand, efficiency can also be increased using bulk micromachining techniques. A different approach to obtain good efficiency values is to use non-standard materials for antenna substrate. Using this approach, it is possible to use materials like BCB, quartz, glass, or artificial substrates. Another attractive option is to use ceramics for the antenna substrate. It has a high dielectric constant, which allow further size reduction and can be found with low losses. The attempts made so far to use ceramics are based on the LTCC technology or in the use of a ceramic package to place the antenna.

Antenna Types

A good substrate material is essential to obtain an antenna with good radiation properties. However, finding a good substrate is only part of the solution. Also critical, is the antenna type selection. It must be small to fit in a small chip area, it should be easy to design, fabricate and characterize, and it should interfere as low as possible with the remaining circuitry. Notwithstanding all the requirements, mainly two types of antennas have been suggested for integration – patch and dipole or monopole antennas. Those antennas have been chosen mainly due to their simplicity to design and to interface with the RF front-end. Nevertheless, even if in a small number, slots, loops, and other types have also been proposed. Another antenna very popular for miniaturization is the slot antenna.

Antenna Integration

Also important, is how the antenna is integrated with RF front-end: on-package, on-chip, or on-wafer. Integration on-package is a very straightforward concept where the chip package is used for antenna housing. Despite the great advantage of using, for free, a dummy package for antenna placement, it also shows some disadvantages. The use of package as antenna substrate requires a good control of the electrical properties of the package material, the package becomes more complex since its necessary to provide feeding to the antenna, and the advantage of integration gets lost a bit since what we get is more an antenna connected on-chip then an antenna integrated on-chip. On-chip integration is the easiest, simplest, and used more often since the antenna is simply designed to operate on the same substrate as the circuitry. However, despite its simplicity, this solution has to deal with the usual low efficiencies obtained. Moreover, noise coupling to and from RF circuitry, interference with RF passive components, such as inductors, is still lacking analysis. Also very important, this approach consumes very expensive chip area.

On-chip Antennas

The integration of antennas requires the availability of simple, small, and efficient antennas that can be designed and fabricated with techniques and materials compatible with IC processing. Since the substrate materials available for integrated circuits fabrication were not chosen to design antennas on it, first it’s necessary to characterize those substrates and find the most suitable one for this purpose.

Substrate Characterization

Several different methods can be used to extract the electrical intrinsic properties of a material. From the most widely used techniques to obtain those properties in the microwave region, the transmission line technique is the simplest method for electromagnetic characterization in wideband frequencies [15, 16]. The S-parameters measurements of a planar test cell can be used to obtain the desired parameters, where either a microstrip or a coplanar waveguide (CPW) can be used as test cell.

In this work, the CPW was used, with its parameters chosen to allow only the dominant quasi-TEM mode to be present. For on-wafer measurements the CPW, without bottom ground, is the easiest structure to feed and the probe station tips are able to touch directly the CPW lines. The S-parameters are then easily measured with a vector network analyzer.

Extraction Method

The electrical properties were obtained from the S-parameters measurements of a planar transmission line test-cell. The coplanar waveguide was used because of the possibility to define a planar shape that can propagate a dominant mode (quasi-TEM). In the case of dominant mode, the coplanar characteristic impedance is quasi-constant in a broad frequency range, for a large variety of substrates and a cell structure obeying $h > W + 2S$ [15]. This cell has also the advantage of avoiding the use of vias to ground.

The CPW cell geometry used for S-parameter measurements is shown in Fig. 3.

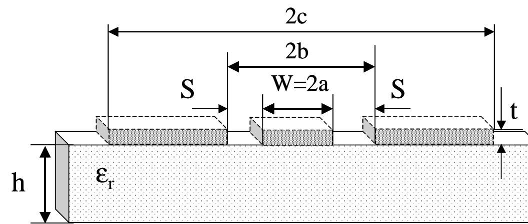

Figure 3. CPW cell used for S-parameters measurement.

The effective dielectric constant for this type of CPW can be obtained from [15]:

$$\varepsilon_{reff} = -\left(\frac{-\ln T}{\omega d \sqrt{\varepsilon_0 \mu_0}} \right)^2 \tag{1}$$

where ω is the angular frequency, ε_0 and μ_0 are the free space permittivity and permeability, d is the coplanar line length and T is the first transmission coefficient. The transmission coefficient can be obtained from the measured scattering parameters using the following equation [16]:

$$T = \frac{S_{11} + S_{21} - \Gamma}{1 - (S_{11} + S_{21})\Gamma} \tag{2}$$

with

$$\Gamma = \mathrm{X} \pm \sqrt{\mathrm{X}^2 - 1} \tag{3}$$

and

$$\mathrm{X} = \frac{S_{11}^2 - S_{21}^2 + 1}{2S_{11}} \tag{4}$$

The electrical permittivity is obtained from the equations characterizing a coplanar waveguide with finite-width ground planes [17]. In this way, the effective electrical permittivity is given by:

$$\varepsilon_{reff} = 1 + \frac{1}{2}(\varepsilon_r - 1)\frac{K(k)}{K(k')}\frac{K(k_1^{'})}{K(k_1)} \tag{5}$$

where ε_r is the relative permittivity of the substrate, K is the complete elliptical integral of the first kind and $k' = \sqrt{1-k^2}$ [18]. The arguments k and k' are dependent on the line geometry and are given by [19]:

$$k = \frac{c}{b}\sqrt{\frac{b^2 - a^2}{c^2 - a^2}} \tag{6}$$

and

$$k_1 = \frac{\sinh(\pi c/2h)}{\sinh(\pi b/2h)}\sqrt{\frac{\sinh^2(\pi b/2h) - \sinh^2(\pi a/2h)}{\sinh^2(\pi c/2h) - \sinh^2(\pi a/2h)}} \tag{7}$$

The characteristic impedance of the coplanar cell can also be computed from the measured S-parameters [20]:

$$Z_c^2 = Z_0^2 \frac{(1+S_{11})^2 - S_{21}^2}{(1-S_{11})^2 - S_{21}^2} \tag{8}$$

where Z_0 is the reference impedance (50 Ω).

To compute the attenuation, its necessary to obtain the propagation constant $\gamma = \alpha + j\beta$ for the CPW cell. This can be computed by means of [21]:

$$e^{-\gamma l} = \left\{ \frac{1 - S_{11}^2 + S_{21}^2}{2S_{21}} \pm K \right\}^{-1} \tag{9}$$

where

$$K = \left\{ \frac{(S_{11}^2 - S_{21}^2 + 1)^2 - (2S_{11}^2)^2}{(2S_{21}^2)^2} \right\}^{\frac{1}{2}} \tag{10}$$

Attenuation in microwave lines occurs due to radiation, metal and substrate losses. Assuming that radiation losses are very small, it's possible to obtain the dielectric loss tangent from the value of the total attenuation and conductor losses.

The attenuation due to conductor losses in the center strip conductor and ground planes of a CPW is given by [22]:

$$\alpha_c \approx \frac{R_{sm} b^2}{16 Z_0 K^2(k)(b^2 - a^2)} \cdot \left\{ \frac{1}{a} \ln\left(\frac{2a}{\Delta} \frac{(b-a)}{(b+a)} \right) + \frac{1}{b} \ln\left(\frac{2b}{\Delta} \frac{(b-a)}{(b+a)} \right) \right\} \tag{11}$$

with

$$R_{sm} = \omega \mu_c t \, \mathrm{Im}\left(\frac{\cot(k_c t) + \csc(k_c t)}{k_c t} \right) \tag{12}$$

where k_c is the wave number, ω the angular frequency and μ_c the permeability of the conductor.

From the knowledge of the total and metal losses we can obtain the dielectric loss tangent from the attenuation constant due to the dielectric losses [18]:

$$\alpha_d = \frac{\pi}{\lambda_0} \frac{\varepsilon_r}{\sqrt{\varepsilon_{eff}}} q \tan \delta \tag{13}$$

where q is the filling factor that depends on the geometry.

Next, the description of the test cells required to measure the S-parameters is presented.

CPW Cells Design

Because the substrate losses are relatively small, lines with 5-mm length were used to increase the calculations accuracy. The metal areas were fabricated with a 2 µm layer of aluminium on top of each wafer. A sample of the fabricated lines is shown in Fig. 4. Since the exact electrical permittivity value at the desired frequencies was not known, several CPW cells were designed in order to obtain a suitable configuration for the material properties extraction. It is recommended the use of some mismatch in order to obtain a good accuracy [15]. In this way, the CPW cells were designed with different *W/S* ratios in order to obtain different characteristic impedances. Namely, lines with the following dimensions were used:

(W = 75 μm, S = 15 μm), (W = 50 μm, S = 35 μm), (W = 75 μm, S = 50 μm) and (W = 100 μm, S = 60 μm).

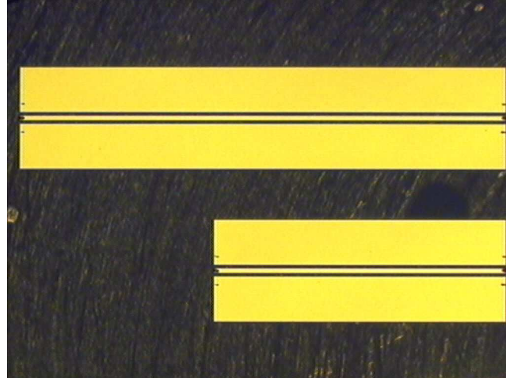

Figure 4. Sample of the fabricated coplanar waveguides used for S-parameter measurement.

Materials Properties

The measured S-parameters of a coplanar waveguide (CPW) propagating the dominant mode were used to obtain the electrical permittivity and the dielectric loss tangent of three different glass wafers: non-alkaline Schott AF45, Corning Pyrex #7740 and Hoya SD-2. These properties were obtained up to 10 GHz. A vector network analyzer and a probe station were used to perform the on-wafer measurements of the two-port network S-parameters. It was calibrated by means of TRL method, providing a measuring reference plane at the edge of the coplanar lines.

Glass Wafers Characterization

The electrical permittivity is presented in Fig. 5 for the three glass wafers under. As can be seen from that figure, for high frequencies, and as expected, the electrical properties show only a slight variation with frequency. Also, we can observe an abrupt change on the measured characteristics at low frequencies. This happens because at those frequencies the assumptions behind the theoretical formulation are not anymore valid. At the frequencies of interest (5-6 GHz), the dielectric constants for SD-2, borofloat and AF45 are 4.7, 5.9 and 6.1, respectively.

The losses are difficult to obtain since they are relatively small for such line lengths. The results can change significantly from one measurement to another, if not enough attention is paid when the contact between probes and lines is established. To compute loss values, the remaining data after discarding the inaccurate measurements were again submitted to a new selection. Only the ones giving the lower values for the losses were used. It was considered that the higher losses were due to imperfect contacts between probes and CPW cells.

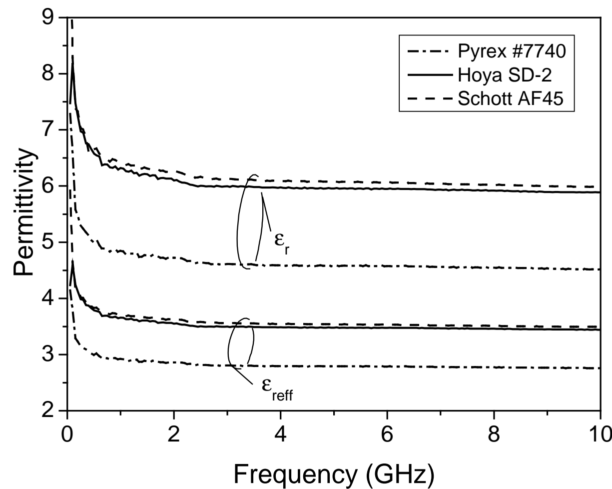

Figure 5. Measured permittivity for three glass wafers.

In Fig. 6, the total attenuation measured in a CPW cell is plotted together with the attenuation due to conductor loss, computed from equation 11. Assuming the radiation losses being very small, the difference between total losses and conductor losses give us the substrate losses.

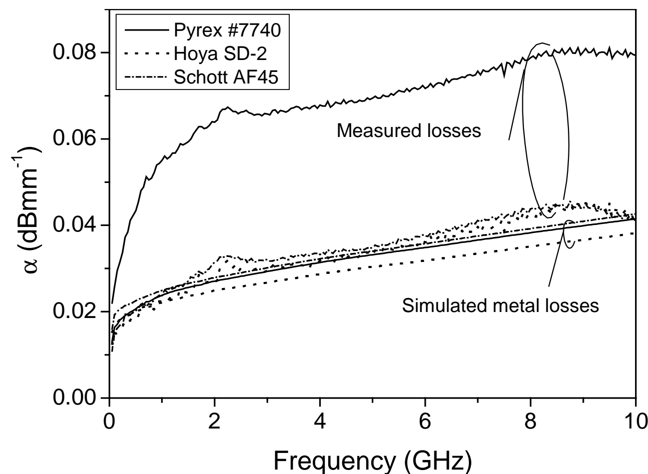

Figure 6. Computed and measured attenuation of a CPW cell with $W = 75$ µm and $S = 50$ µm.

From the above figure we can see that the SD-2 and AF45 substrates suffer from almost the same losses, but the #7740 substrate suffer from increased losses. When designing RF and microwave elements, the structures on the Pyrex and AF-45 wafers should be similar but not the device losses.

The data from Fig. 6 was used to compute the loss tangents. The obtained results are plotted in Fig. 7. As expected from total losses, the SD-2 and AF45 wafers show similar values, and Pyrex wafer presents a higher value for the loss tangent. When possible, AF45 should be used instead of Pyrex #7740.

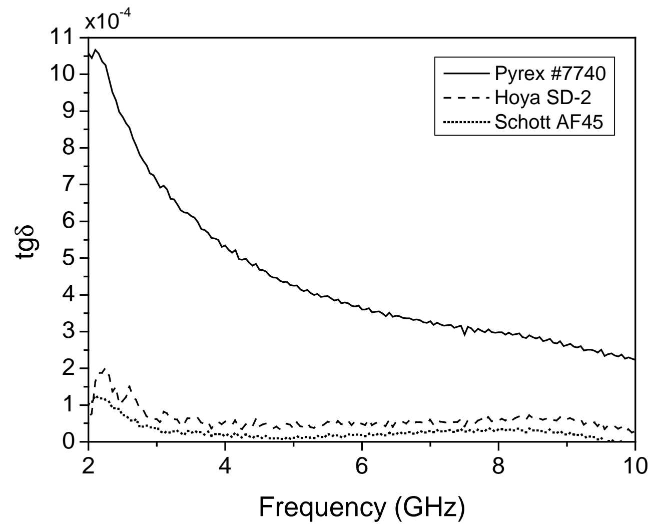

Figure 7. Measured loss tangent (W=75 µm, S=50 µm).

High-resistivity Polycrystalline Silicon

The electrical permittivity of HRPS was also obtained from the measured S-parameters and is displayed in Fig. 8. This plot shows the results obtained from the three different CPW cells. As can be observed in that figure, for high frequencies, and as expected, the electrical properties show only a slight variation with frequency. Also, we can observe an abrupt change on the measured characteristics at low frequencies. This happens because at those frequencies the assumptions behind the theoretical formulation are not anymore valid. At the frequencies of interest (5-6 GHz), the obtained dielectric constant is $\varepsilon_r \approx 11.5$.

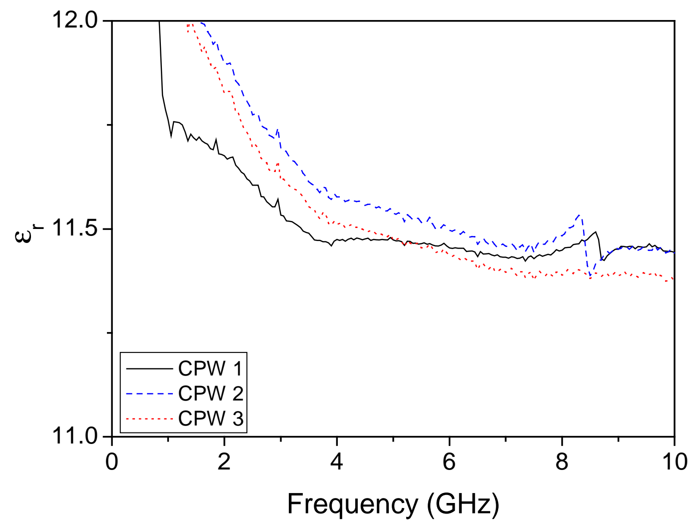

Figure 8. Extracted electrical permittivity for three different CPW cells.

Together with dielectric constant, loss tangent is also a fundamental parameter as it represents the performance achievable with the designed passives. The results obtained for loss tangent are plotted in Fig. 9. As expected, all the CPW lines show similar values since the substrate is always the same.

The method used to obtain the data in Fig. 8 is based on the measured total losses coming from the CPW lines. Then, assuming no radiation losses, it is possible to identify the metal losses and substrate losses. In this way, it is important to refer that the obtained values for loss tangent are heavily dependent on the models used to describe the losses in these kinds of transmission lines.

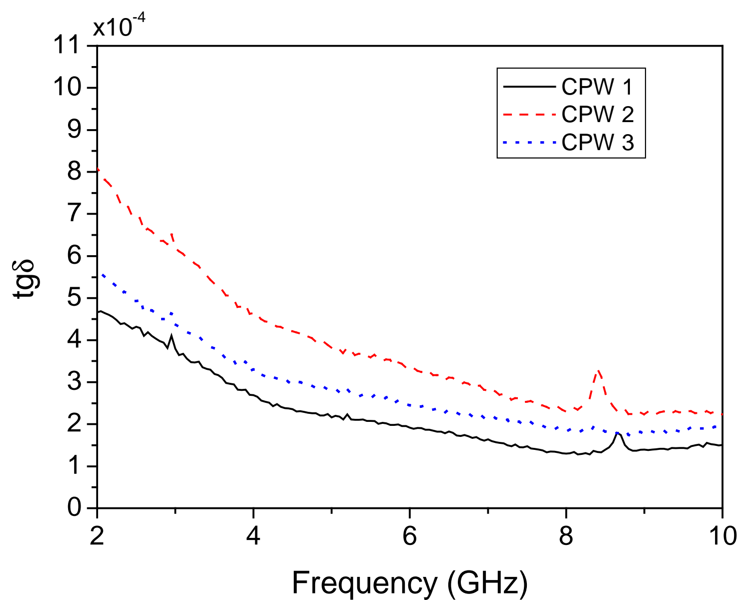

Figure 9. Extracted loss tangent for three different CPW cells.

Patch Antennas

One of the simplest structures that can be used as an integrated antenna is a patch antenna. It is planar and can be fabricated using only two metal layers, one to form the ground plane and other to form the radiating element.

The next antenna design was performed with 3D models built using a 3D FEM simulator tool. The layout was then obtained with the standard IC layout tools. From the set of available materials compatible with IC fabrication, standard silicon was not chosen for use as substrate due to its low resistivity. The option was to use HRS together with insulating layers, to keep the losses as low as possible, and HRPS. Since the antenna dimension is related with its electrical length, which is inversely proportional to the operating frequency, we have chosen to start the antenna design for operation in the 5-6 GHz ISM band. This is an available free band where the antennas can be relatively small and still achieving a good range.

Patch Antennas Using HRS

To obtain the smallest antennas it was used the material with the highest electrical permittivity. Fig. 10 shows the cross-section of the stacked materials with the configuration used in the fabrication.

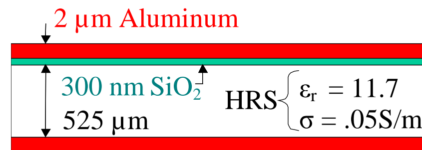

Figure 10. Cross-section view of the realized patch antenna on HRS substrate.

The patch antenna design was supported with a model built using a high frequency structure simulator based on finite elements modeling (FEM) (Fig. 10). A tool with 3D modeling capabilities was necessary due the fact that, for small ground planes, the antenna behavior depends on the ground size.

The two critical steps in designing the patch antenna were the definition of the patch dimensions and the feeding configuration. The patch dimensions have direct influence on the operating frequency and on the antenna gain. The difficulty to predict accurately the patch dimensions is related to the fringing fields together with the small size of the ground plane used. The starting value used for the antenna length, *L*, was half wavelength in the substrate, which is known to give a close value for the operating frequency. This value was then trimmed by simulation.

The antenna feeding should be designed carefully since it must provide a correct impedance matching. At high-signal frequencies it is necessary to design a feeding line with specific characteristic impedance. Also, that line must be connected in a point of the antenna where the input impedance is the same than the feed-line characteristic impedance. The patch antenna was fed with a microstrip line connected to a point inside the patch where the input impedance matches 50 Ω. This connection was achieved with an inset, which had to be properly adjusted with the help of the antenna model.

The model, as well the projected antenna dimensions, is presented in Fig. 11.

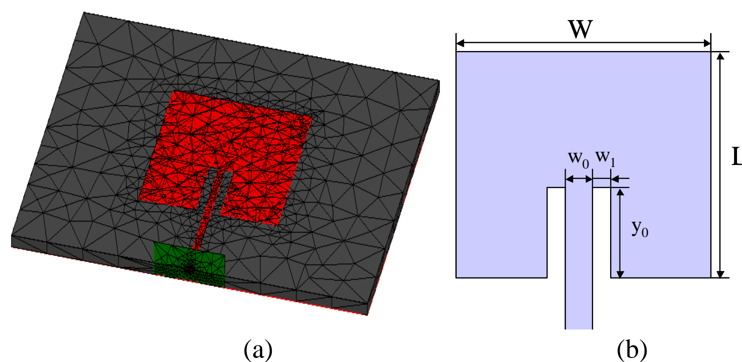

Figure 11. FEM meshed model (a), and layout (b) describing the studied square patch antenna ($L = 7.7$, $W = 7.6$, $y_0 = 3.1$, $w_0 = 0.36$, $w_1 = 0.32$, in mm).

Fig. 12 shows several different patch antennas standing on the top of a HRS wafer. The HRS substrate shown has a dielectric permittivity of 11.7, conductivity in the range of 0.02-0.05 S/m, and the wafer thickness is 525 ± 25 µm. A 300 nm layer of thermal silicon dioxide layer between the silicon substrate and the metal patch was used for insulation. This layer has an ε_r of 3.9 and for design purposes it is assumed to be an insulator. The metal patch and ground plane were obtained using a 2-µm layer of aluminum. Instead, copper could be used to further reduce the metal losses.

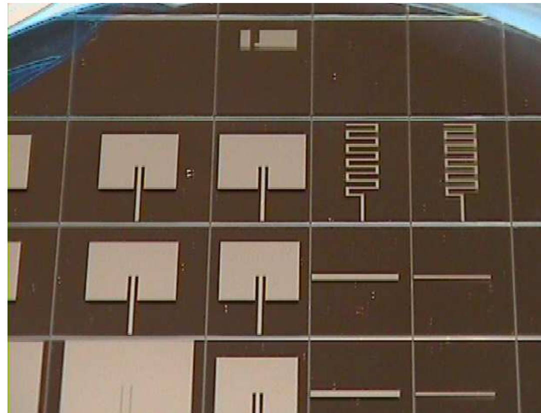

Figure 12. Patch antennas fabricated on a HRS wafer.

To measure the antenna characteristics, it was interfaced with a 3.5 mm coaxial connector. This was achieved by placing the die containing the patch antenna on top of a PCB board with the coaxial connector soldered underneath. One fabricated prototype, ready for measurements, is shown in Fig. 13.

Figure 13. A 7.7x7.6 mm^2 patch antenna realized on a HRS substrate ready for reflection measurements.

All the return loss measurements were performed using an HP vector network analyzer, which was previously calibrated with one-port calibration. The antenna operating frequency, bandwidth, and efficiency were obtained from those return loss measurements.

The simulated and measured values for the patch antenna using HRS substrate are plotted in Fig. 14. The simulated data shows good agreement with the measurements. The obtained operating frequency was 5.705 GHz, providing a -10 dB return-loss bandwidth of 90 MHz.

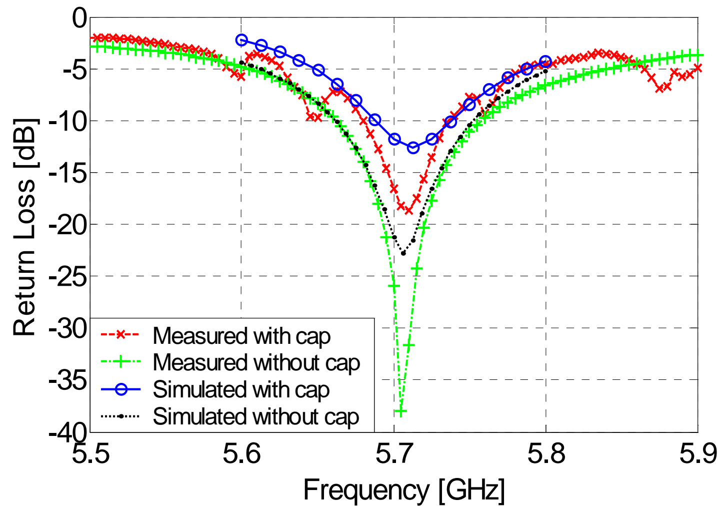

Figure 14. Measured and simulated return loss versus frequency used to obtain the operating frequency, bandwidth and efficiency.

The antenna efficiency was measured using the Wheeler cap method. This method is based on the measurements of the antenna input return loss when it is radiating or not radiating. The last condition is usually met with a metallic cap enclosing the antenna under test. With those measurements the efficiency can be easily computed. The antenna efficiency was also obtained from simulations and compared with the measured values. Using the data from measurements, it was obtained an efficiency of 18.6 %, which is in good agreement with the value computed by the 3D model, that was 19.6 %.

The suitability of an antenna to be integrated depends also on its gain and radiation pattern. The antenna should contribute to a good wireless link range and should not interfere with the already on-chip sensors and electronics. This requires the antenna to radiate mainly in the upward direction, with the backside lobe as weaker as possible. The radiation to the backside can be reduced if the ground plane is big enough. However, all the antenna components should be as small as possible, including the ground plane. The far-field gain patterns measurements were obtained using an anechoic chamber facility. The results are plotted in Fig. 15.

As it was expected, the patch antenna exhibits a linear polarization characteristic, and as it was desired the power is mainly radiated upwards. Nevertheless, it would be desirable to further decrease the power level at the back of the antenna to keep the interference with backside components as low as possible. This drawback results from the small size of the

ground plane. The maximum gain registered was ~0.3 dB. This small gain is essentially due to low efficiency of the antenna, since the substrate suffers from high losses.

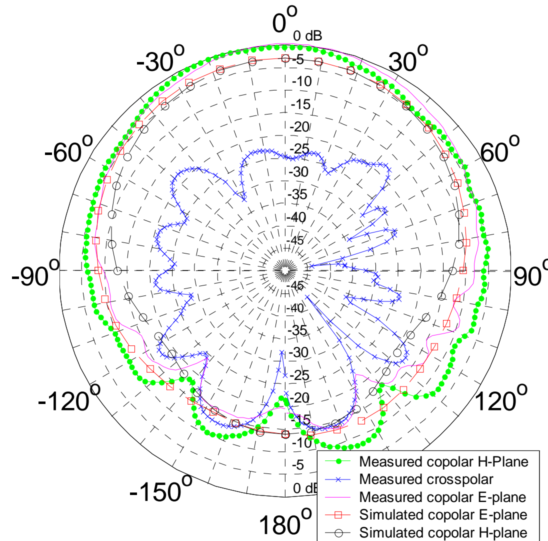

Figure 15. Measured and simulated co-polar and X-polar far-field gain patterns obtained at 5.705 GHz.

After model validation by the measured data, the influence of a few material tolerances were analyzed by simulation. Substrate thickness, substrate conductivity, and oxide thickness were studied. It was observed that varying the substrate thickness from 500 μm to 550 μm and the oxide thickness from 1 μm to 10 μm, the operating frequency changed from about 5.7 GHz to 5.85 GHz. If the substrate conductivity increases from 0.02 S/m to 0.05 S/m, the efficiency decreases from 30.1 % down to 19.6 %.

Patch Antennas on HRPS

The fabrication of patch antennas on HRPS followed a similar process than the antennas fabricated on HRS. The patch antenna was also designed for fabrication on top of an HRPS wafer, without any insulating layer between the metal patch and the substrate. The antenna was designed to operate in the 5-6 GHz ISM band, which yields antenna dimensions of 7.7x7.6 mm^2. The patch metal layer was made with 2 μm of sputtered aluminum and the feeding was realized through a microstrip line.

The measured values used in the Wheeler cap method are plotted in Fig. 16. The figure shows measured values when the antenna is radiating and when it is not. Using the data from measurements, it was obtained an efficiency of 25.6 %, which is in good agreement with the value computed by the 3D model, that was 28.6 %.

It was also verified that this antenna has an operating frequency of 6.25 GHz, with a -10 dB return loss bandwidth of ~200 MHz.

For comparison, a similar patch antenna was fabricated on a Pyrex #7740 wafer. Similarly, 2 μm of sputtered aluminum were used to obtain the metal patch layer. Such antenna has a measured operating frequency of 5.995 GHZ and the -10 dB return loss

bandwidth is ≈100 MHz. From the measurements we obtained an efficiency of 51%, which is higher than the obtained with HRPS. The drawback is the increase in the antenna size.

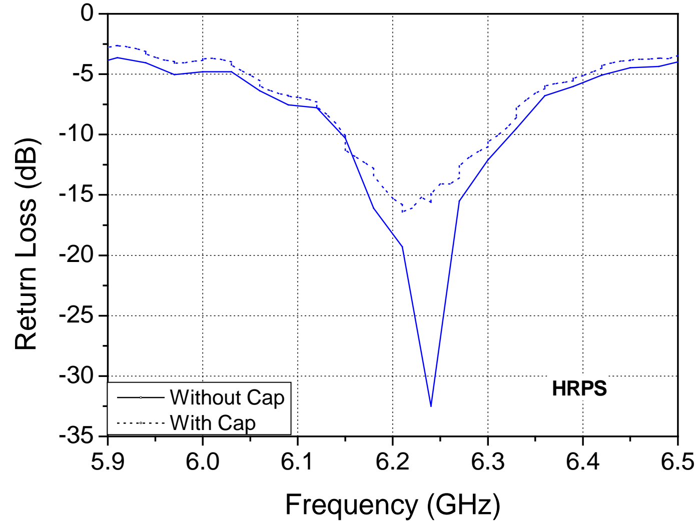

Figure 16. Measured return loss versus frequency used to obtain the operating frequency, bandwidth and efficiency.

MEMS Micro-Antennas

What is the challenge to design wireless communications for biomedical applications? At a first glance, if we make a quick survey in the available databases, it seems that there is no problem since it is not easy to find many references to this topic. However, in previous sections, it was already shown the difficulty in the design of integrated antennas. In this section, the fundamental limits will be revisited and solutions will be discussed to achieve smaller antennas.

Electrically Small Antennas

The physical dimension of the host microsystem limits the available room for antenna integration. In this way, the antenna must be as small as possible, including the ground plane dimensions. This has several implications in the antenna performance and in the neighbour circuits.

Fig. 17 shows the antenna integration using wafer-level chip-scale packaging (WLCSP), together with radio-frequency passives. To save space, the antenna is placed on top of the active circuits. Nevertheless, since the antenna ground plane is very small, not exceeding the antenna dimensions, the system performance is affected.

The antenna is very close to the circuits, allowing a possible coupling between it and any passive devices (inductors or transmission lines). The perfect solution is to obtain an antenna small enough to grant extra space for an antenna ground plane larger then the antenna itself.

Several small and planar antenna types have been proposed for wireless communications [23], but none of them was designed to fulfill all the restrictions and requirements set by on-chip integration. Those restrictions include the properties of available substrate materials and the way they can be processed. Many of the previously proposed solutions to integrate antennas on-chip have been based on the design of planar antennas using silicon as substrate. Since the low-ohmic silicon substrate suffers from high losses, high-resistivity silicon or bulk micromachining have to be used in order to increase the antenna efficiency. Nevertheless, the afore-mentioned solutions have the drawback of increased cost, and the micromachining solution have also the penalty of large area used for antenna implementation. In this way, a preferable solution to decrease the antenna losses may be to use a combination of a low-loss material with silicon. The new material can be used as antenna substrate and any required high-quality factor passives [24], and the silicon will be used to implement the necessary circuitry.

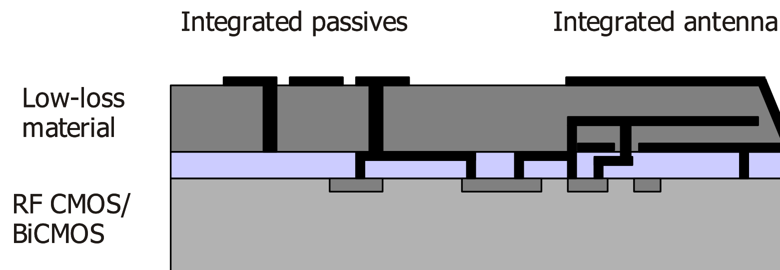

Figure 17. Envisioned application of WLCSP for antenna and other passives integration.

The combination of materials may be achieved with the use of WLCSP techniques, like adhesive wafer bonding and through-wafer electrical via formation, which allows the use of silicon together with different silicon-compatible substrates [25]. However, typical silicon-compatible substrates (e.g. glass, BCB, polyimide, SU-8) have lower dielectric constant compared to silicon. In this way, the use of such materials reduces the losses at the expense of a size increase in the integrated antenna. Therefore, the use of an advanced antenna design may be required to overcome this drawback, providing a small and effective radiator.

In our previous work [26] and other related work [27], the use of shorted-folded patch antennas was considered as a solution to obtain a small antenna. Notwithstanding the obtained success, the dimensions of the developed antenna are still rather large.

Fundamental Limits

A common question asked when the antenna miniaturization is required is: “What is the theoretical limit for antenna size reduction?”. The first work trying to answer this question dates back from 1947 [28]. In that work, Wheeler investigated the fundamental limits of electrically small antennas. An electrically small antenna was defined to have overall dimensions smaller then $\frac{\lambda}{2\pi}$. Sometimes, this is also referred under the relation $ka < 1$, where $k = \frac{2\pi}{\lambda}$, where λ is the free space wavelength and a the radius of the smaller sphere

enclosing the antenna, also called the radian-sphere. Fig. 18 shows the concept widely adopted to characterize an electrically small antenna.

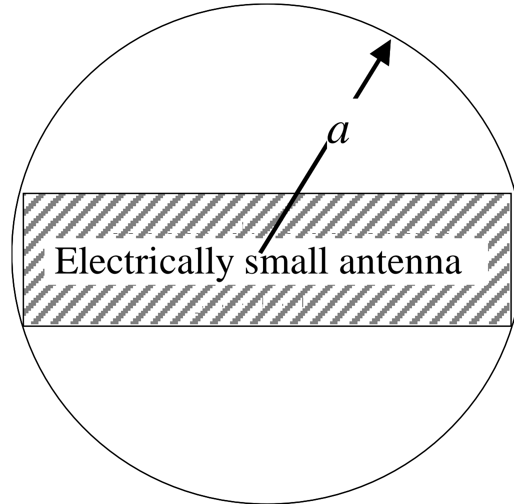

Figure 18. Electrically small antenna enclosed by the radian-sphere.

In his work, Wheeler analysed which could be the highest efficiency of an electrically small antenna, considering it as a capacitive or inductive load. Some time later, Chu published his work about electrically small antennas [19]. In that work, spherical wave functions were used to describe the antenna field, gain, and quality factor. One research topic was to find the maximum gain achievable by an antenna of moderate complexity. This is equivalent to find the minimum quality factor for the antenna. Other research topic was to find the maximum ratio gain/quality factor.

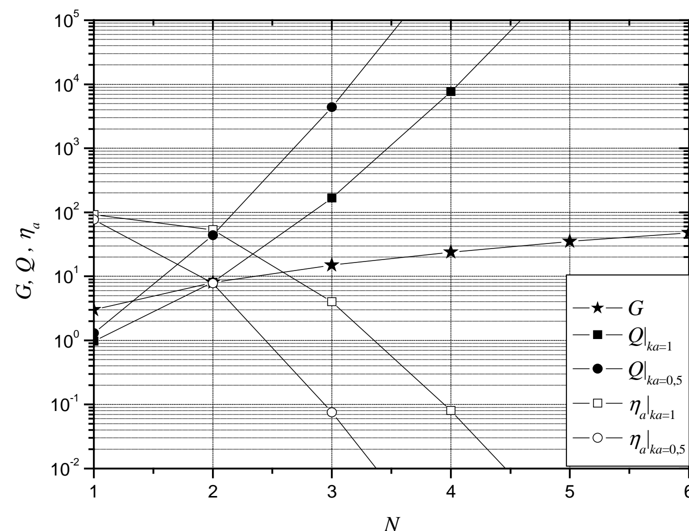

Figure 19. Tradeoffs in antenna parameters as a function of antenna complexity, *N*.

From there on, Chu results have been widely used as a reference in antenna size reduction. Several authors have since then studied the behaviour of electrically small antennas [30-40]. From those studies it is possible to conclude that, theoretically, it is possible to obtain an antenna with an extremely high gain. However, there are other important parameters in an antenna, namely efficiency and quality factor (bandwidth).

Fig. 19 shows the tradeoffs in antenna parameters as the antenna complexity, *N*, increases, for two antenna dimensions. It can be observed that the gain, *G*, and quality factor, *Q*, increases with the antenna complexity, and the efficiency, η_a, is reduced. It can also be observed that the larger antenna has a smaller quality factor and a larger efficiency.

Other interesting analysis is to observe the behaviour of antenna quality factor, efficiency, and gain for an antenna operating in the fundamental mode. Fig. 20 shows the results of such analysis, where it can be observed that all antenna parameters are improved as the antenna dimension increases. It can also be observed the fast degradation of antenna efficiency for $ka < 0.4$.

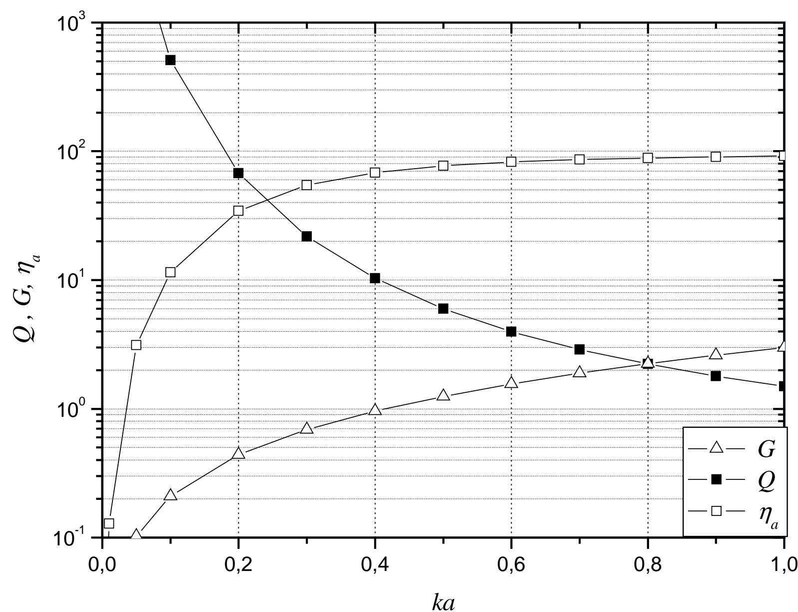

Figure 20. Influence of antenna dimensions on gain, quality factor, and efficiency.

Wafer Level Packaging

The properties of a small antenna are dependent on how it fills it radian-sphere [40]. This means a dipole antenna will have worst properties then a patch antenna, since the patch antenna uses more space inside the radian-sphere. In this way, a very attractive option is the antenna integration using stacked wafers, where the antenna uses not only two dimensions, but also a third dimension, at a reduced cost.

The technical solution for this integration approach is the application of wafer-level chip-scale packaging (WLCSP) techniques. This approach represents a truly added value as at a limited cost 3D passive structures can be realized without increasing the chip active

dimensions. Also, WLCSP allows combination of a different substrate (e.g. HRS, glass) together with low-ohmic silicon. The use of new wafer materials may reduce the losses with the potential of allowing the integration of other passive devices. Moreover, the possibility to fabricate 3D structures allows the implementation of more advanced antenna structures, where size and efficiency restrictions may be met more easily. Fig. 21 shows two options on how to use the WLCSP concept to integrate antennas and/or other passive devices.

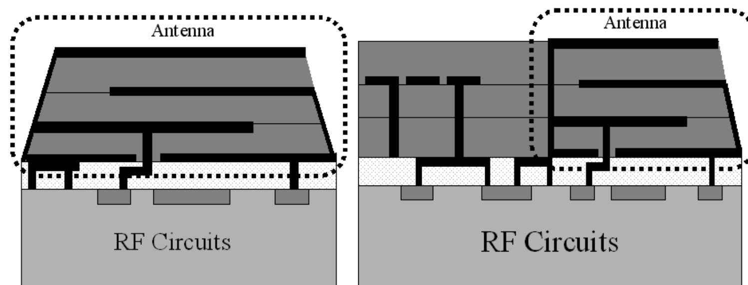

Figure 21. Integration of a small size antenna with RF circuitry.

In the next section, we will introduce the use of WLCSP for integration of planar antennas built using silicon compatible substrates. The suitability of folded patch antennas, built on HRS and glass, are investigated as candidates for on-wafer integration. The 3D antenna models were built and the measured antenna parameters were compared with the values obtained by simulation. Despite its higher fabrication complexity, the folded patch antenna has an increased performance when compared with the patch antenna, and at the same time allows reduction of the used chip area. In this way, the use of glass substrate enables a small on-wafer antenna and RF electronics direct coupling. This offers potential of low cost, low profile and simplified assembly.

Folded-patch Antenna

The possibility to integrate on-chip antennas for biomedical devices is highly dependent on the achievable antenna dimensions and efficiency. Reduction of dimensions together with efficiency improvement can be obtained through proper device geometry. Since the patch antennas are rather large for on-chip integration, the use of a shorted-folded patch antenna on glass was considered.

Antenna Modelling

The proposed, on-chip integrated, folded short-patch antenna (FSPA) is shown in Fig. 22. It consists of three horizontal metal sheets that are electrically connected by two vertical metal walls.

All structure is embedded in a dielectric substrate having certain electrical permittivity and dielectric losses. These two parameters together with the antenna geometry and its actual dimensions will determine its radiation characteristics and overall performance.

For the best performance, the metal sheets should have minimum resistivity and the dielectric should be a low-loss material, which allows high efficiency. Also, to achieve small

antenna dimensions, a substrate with high electrical permittivity is desirable. High antenna efficiency requires thicker substrates (>300 μm) and therefore high aspect ratio vias in glass are required.

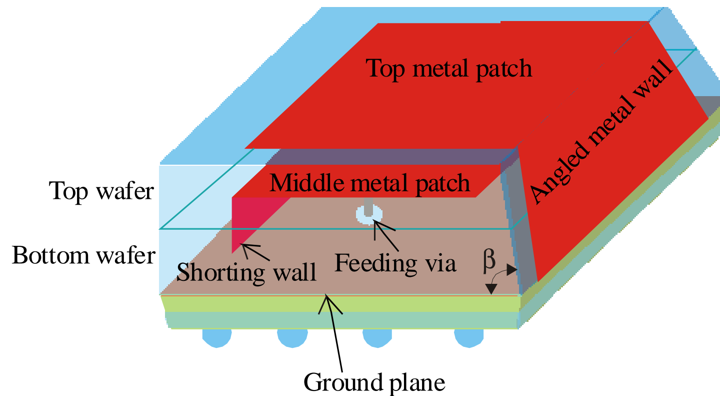

Figure 22. Proposed shorted-folded patch antenna.

At frequencies above 1 GHz, glass becomes a very attractive option. Its main advantages are low losses, reasonable ε_r, availability in a form of wafers with any required thickness and diameter, and last but not least low cost. There is also sufficient experience in processing of glass wafers from MEMS and WLP applications.

The antenna was designed to operate at 5.7 GHz, a frequency chosen to be inside the 5-6 GHz ISM band. All the simulation analysis was performed with an antenna model that was built using the High Frequency Structure Simulator from Ansoft, a 3D tool based on finite element modeling. This simulation tool was intensively used previously in our patch antenna design, where good match of modeling and experimental results were achieved. The developed antenna model is displayed in Fig. 23.

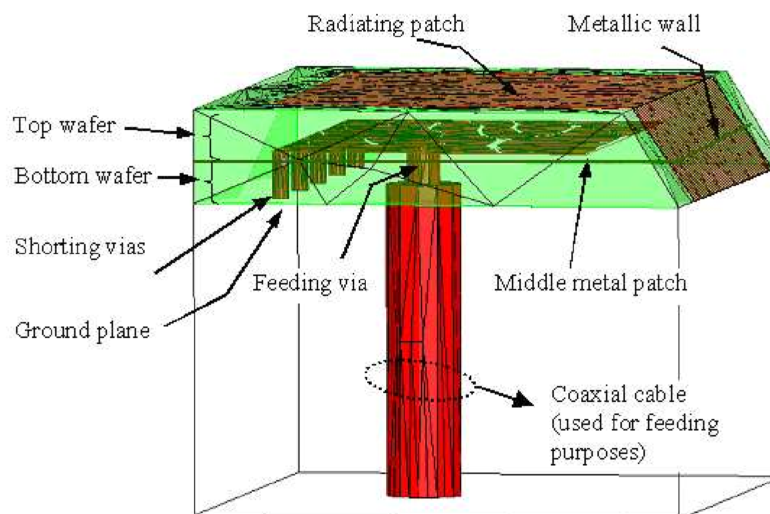

Figure 23. 3D FEM model of the fabricated folded shorted-patch antenna.

From the fabrication point of view, it is preferable to keep the overall antenna thickness small. To achieve this, thin or thinned wafers can be used. However, the wafer thickness is a relevant parameter that influences the antenna performance, since it corresponds to the antenna substrate thickness. To study this effect, all the FSPA dimensions were kept constant, except the wafer thickness, *h*, which was as a parameter. The obtained results for the return loss are presented in Fig. 24.

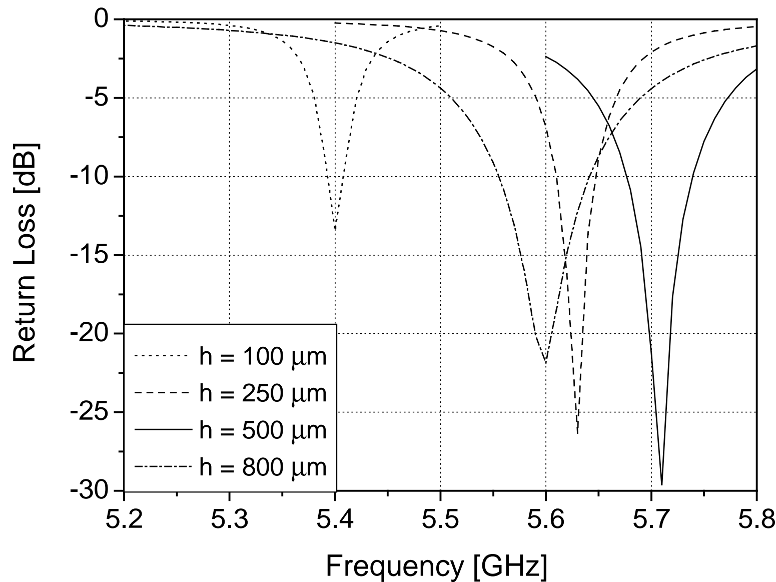

Figure 24. Return loss of the FSPA for different substrate thickness values.

It can be observed that decreasing the wafer thickness from 500 μm down to 100 μm leads to a reduction of the antenna operating frequency. This is a desirable effect since, for the same operating frequency, the antenna can be smaller. However, a thinner substrate, and thus a smaller volume of the antenna dielectric, will cause reduction of the antenna radiation efficiency as well as reduction of the antenna bandwidth. If the wafer thickness is increased to 800 the operating frequency starts to decrease again, instead of a monotonously increase with thickness increment. In opposition to what we could be induced by observation of Fig. 24, the expected behavior would be a decrease in the operating frequency as the wafer thickness is increased since the electrical length of the antenna becomes larger. However, the gap between the middle patch and the ground plane has a significant effect in the antenna operating frequency. In this particular design, that gap starts to be the dominating effect in setting the operating frequency when the wafer thickness is more then 500 μm, which explains the frequency decrease with wafer thickness decrease.

Together with the reduction in the antenna dimension and increased efficiency, despite the added cost of fabrication complexity, with this type of antenna the following material combinations can be formed: glass/glass, HRPS/HRPS, or glass/HRPS. An option to avoid the difficult task of doing through-wafer vias in glass could be to replace the glass wafers by HRPS. This will inevitably increase a bit the dielectric losses, but at the same time the antenna dimensions could be reduced. Other option is to substitute only the bottom glass

wafer by HRPS. In this way, the vias in glass are not required and the overall losses are expected to be smaller.

All the proposed options were analyzed based on 3D FEM modelling built using. Considering a 10 kΩ-cm substrate, the predicted results are summarized in Table 1. For various substrate options, the dimensions of the antenna model were kept constant as possible, only some minor adjustments were implemented to adjust the operating frequency and/or to achieve impedance matching.

Table 1. Summary for the different stack options.

	glass/glass	HRPS/HRPS	HRPS/glass
F_c	5.66 GHz	5.66 GHz	5.64 GHz
BW	60 MHz	57 MHz	63 MHz
Eff.	66 %	64 %	65 %
L_1	3.2 mm	1.8 mm	3.2 mm
L	2.6 mm	1.65 mm	2.3 mm

Parameters shown: F_c – operating frequency, BW – bandwidth, Eff. - efficiency, L_1 - top patch length, L - middle patch length.

As can be seen from Table 1, the antenna built on a stack of two glass wafers has the highest efficiency and the largest dimensions. The antenna on a stack of two HRPS wafers is the smallest and has the lowest efficiency. When the glass/HRPS stack is used, a compromise can be obtained. The losses are slightly increased and the dimensions don't change significantly. The antenna dimensions are strongly dependent on the projected efficiency and bandwidth and also on the substrate thickness but, if we use HRPS/HRPS, they can fit inside an area of 3x3 mm^2. The achievable –10 dB return loss bandwidth is around 50 MHz (+/- 10 MHz).

The use of a 10 kΩ-cm HRPS wafer makes on-chip antenna integration possible with an antenna efficiency and electrical performance similar to the one obtained with glass, but with the benefit of a smaller size (12.4x11.7 vs. 7.7x7.6 mm^2 for patch antenna and 4x4 vs. 3x3 mm^2 for folded-patch antenna at 5.7 GHz) since the dielectric constant is two times higher for HRPS. Next to that, the inherent problems associated with glass substrate processing (e.g. difficulty to form high-aspect ratio vias) are avoided.

Antenna Fabrication

Despite the potential of HRPS, it was decided to evaluate the suitability of glass wafers for antenna applications because of its popularity in biomedical diagnostic devices (e.g. lab-on-chip) that may also benefit from on-chip antenna.

The folded-patch antenna fabrication sequence is schematically shown in Fig. 25. Two AF-45, 100 mm diameter and 500 µm thick glass wafers are used as the starting material.

Firstly, 200 µm diameter through-wafer vias were formed in the bottom glass substrate. A laser system at Philips CFT with a 30:1 reduction mask was used for ablation of the feeding and shorting vias. Because the selected glass substrate material exhibits sufficient light absorption in the UV region only, a 193 nm excimer laser was required. The initial tests with 248 nm laser were not successful due to formation of cracks. The vias were then metallized by sputtering of 4µm Al layers from both sides of the wafer. Due to the low aspect ratio of the

vias (2.5:1) and the fact that the sidewalls are not perfectly vertical, it was possible to form a continuous conductive layer within the vias. The middle antenna patch was then patterned using electroplated photoresist and plasma etching (see Fig. 26).

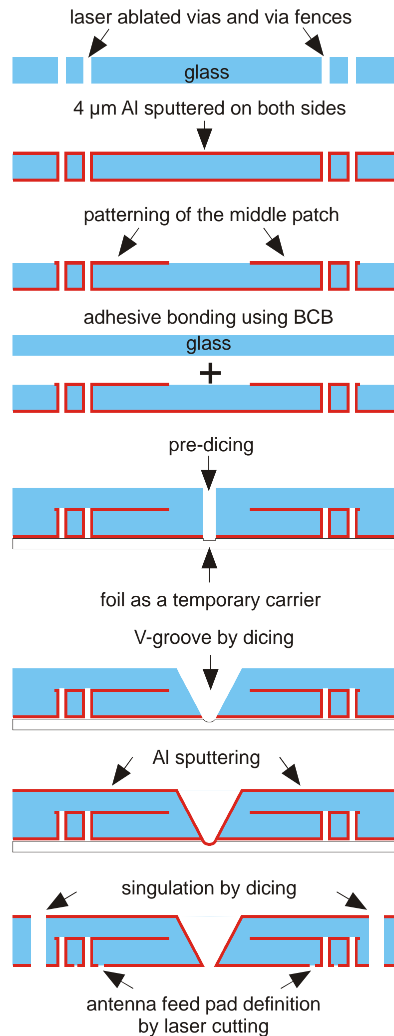

Figure 25. Schematic fabrication sequence used for antenna fabrication.

Then, the second glass wafer was adhesively bonded using ~5-7 µm thick BCB layer as the adhesive. This wafer stack was attached to a temporary carrier (foil or Si wafer) to allow formation of the slanted antenna sidewall by V-blade dicing. The sidewall shaping was performed in two steps. First, a vertical trench through the wafer stack was formed using a 400 µm wide dicing blade. In the second step, a V-shaped dicing blade (60 deg. angle) was applied to shape the antenna sidewalls. The accuracy of this step is critical for antenna electrical properties and care has to be taken to achieve alignment with the middle antenna patch. The achievable accuracy of blade positioning is close to 2 µm, which is more than sufficient.

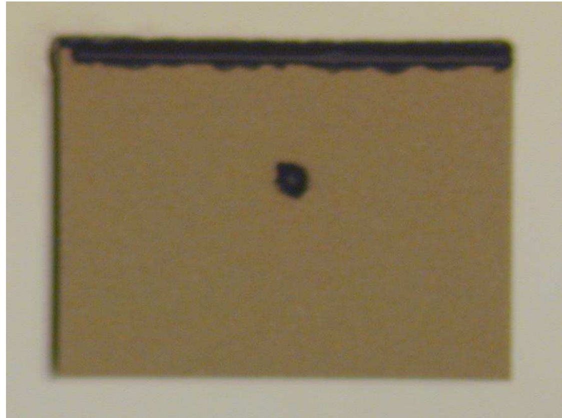

Figure 26. Photograph showing detail of the bottom glass substrate with the 200 μm diameter ablated vias and the patterned middle Al antenna patch.

The antenna fabrication then continues by Al-layer sputtering to metallize the second glass wafer including the V-shaped trenches. Finally, a standard dicing with vertical sidewalls is applied to define the remaining three antenna sidewalls and thus the lateral dimensions of the final antenna. The fabricated antenna prototype, compared to a 1 eurocent coin, is shown in Fig. 27.

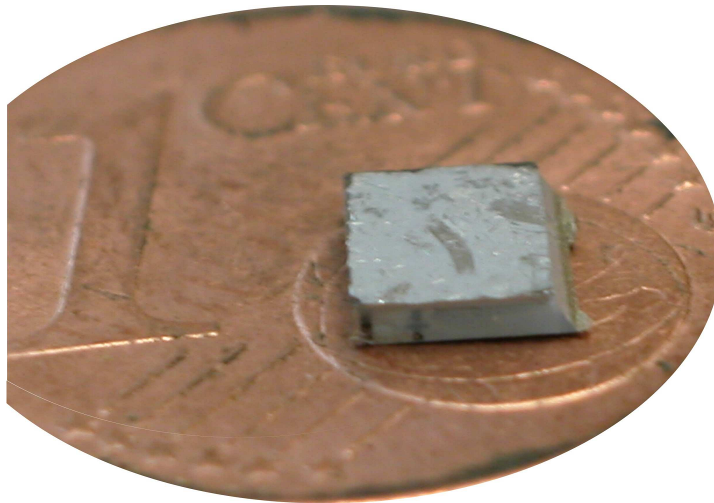

Figure 27. Photograph of the folded shorted-patch antenna prototype realized on a stack of two AF-45 glass substrates.

Antenna Results

For fabrication simplicity, laser cutting on the to-be-measured samples defined the antenna-feeding pad. For the measurement purposes, the antenna was attached to a PCB with a 50 Ω microstrip line, and the antenna feeding pad was connected using multiple bond wire connections (see Fig. 28).

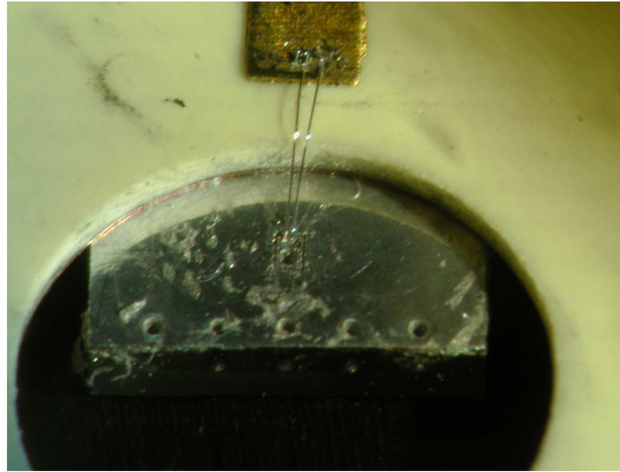

Figure 28. Close-up of antenna backside feeding point connected to a PCB, using multiple bond wires.

A prototype was fabricated with the technique described before, where the laser ablation was used to obtain the through-wafer vias. To measure the fabricated antenna, it was necessary to attach it to a PCB board, where a 50 Ω microstrip line was designed to interface the antenna with a coaxial connector that provides the connection to the vector network analyzer. The connection between the microstrip line and the antenna feeding via was made by wire bonding. The return loss measurements were performed with an E8358A vector network analyzer. Fig. 29 shows the measured and simulated values for a fabricated prototype.

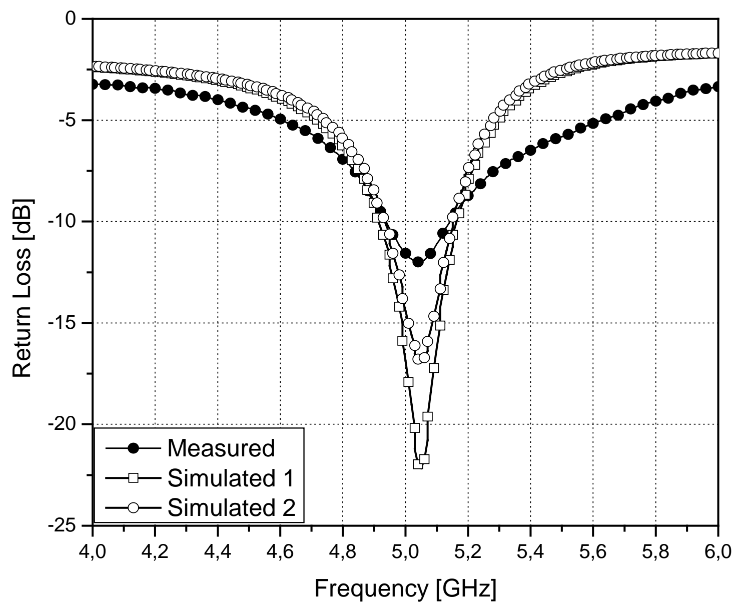

Figure 29. Measured and simulated return loss of the fabricated antenna prototype.

The simulated values on this plot were obtained after antenna fabrication, where relevant process dependent parameters were updated to better match the values obtained during antenna processing. Also, it was included the effect of the ground plane that was used to mount the antenna for simulations. The difference between the projected and measured bandwidth are mainly due to the thickness of the metal inside the shorting and feeding vias, as we were able to verify by simulation. If the metal thickness of vias metallization changes from, e.g., 2 to 0.02 µm it was obtained by simulation that the bandwidth changes from ~50 to ~200 MHz. The small shift in the desired operating frequency from 5.1 to 5.05 GHz is due to a small increase in the dimensions of the top metal patch. This top metal patch was first designed to be defined by patterning but to reduce costs, was defined by the singulation step (Fig. 25), resulting in a larger patch.

The simulated values on Fig. 29 were obtained after antenna fabrication, where relevant process dependent parameters were updated to better match the values obtained during antenna processing. Also, it was included the effect of the ground plane that was used to mount the antenna for simulations. After that adjustment, it was possible to obtain a good agreement between the measured and the simulated data. The final antenna dimensions are 4x4x1 mm^3, the operating frequency is 5.03 GHz with a bandwidth of ~200 MHz.

Cantilever Antenna

From the previous antenna design sections, it is clear that the FSPA shows advantage in occupied area requiring, however, a more complex fabrication process. The dimensions of the FSPA is suitable for small biomedical devices like the required for spinal cord stimulation or for implants used in neural signal recording. The main drawback is that it operates only inside the 5-6 GHz ISM band. This results in high losses in signal propagation inside the human body, requiring placement of the biomedical devices at the body surface. This is not a satisfactory solution for, e.g., human hear implants, or implants required to be inside the spinal cord.

To communicate with those devices its necessary to find a new solution, which will be discussed next.

MEMS Magnetic Sensors

Micro-Electro-Mechanical Systems (MEMS) are an available option for RF communications systems, since they can offer, simultaneously, devices with improved performance and integration capability in a silicon chip, side by side with semiconductor circuits, since they use IC-compatible materials.

The basic principle of micromachined cantilevers offers an interesting possibility to measure a variety of physical parameters [41]. They can be applied as magnetometers for measuring the magnetization [42, 43] and as viscosity sensors [44]. These devices are excited at the resonant frequency to achieve high sensitivity.

Up to now, MEMS have been used in antenna applications, not as an antenna itself, but to obtain non-conventional front-ends with improved, or new characteristics However, it is well known that some MEMS structures can be used as magnetic flux sensors, allowing the detection of time varying fields [45].

When used as a sensor, a MEMS structure requires the use of a sensing mechanism and the most widely used is the capacitive method. The moving structure, and a fixed plate, forms a parallel plate capacitor, where the structure movement is translated into a capacity change. On the other hand, when it has to be used as an actuator, the electrostatic actuation is widely used as the actuating mechanism due to its simplicity. The two main structures used are comb drives [46] and parallel plates [47]. While in the comb drive, which is based on area-varying capacitors, the displacement varies linearly with the gap, in actuators that relies on gap-width varying capacitors (parallel-plate) the pull-in phenomenon has to be considered [47]. Pull-in causes the displacement range due to electrostatic force to be limited to one-third of the gap between the electrodes, in case of a motion perpendicular to the capacitor plate orientation. This effect also limits the dynamic range of capacitive accelerometers operating in the feedback mode. Charge drive (current drive with a series capacitance), rather than direct voltage drive can be used to circumvent pull-in, however, at the expense of attainable maximum force for given device dimensions.

A U-shaped cantilever, proposed to detect a time-varying magnetic field, is presented in Fig. 30.

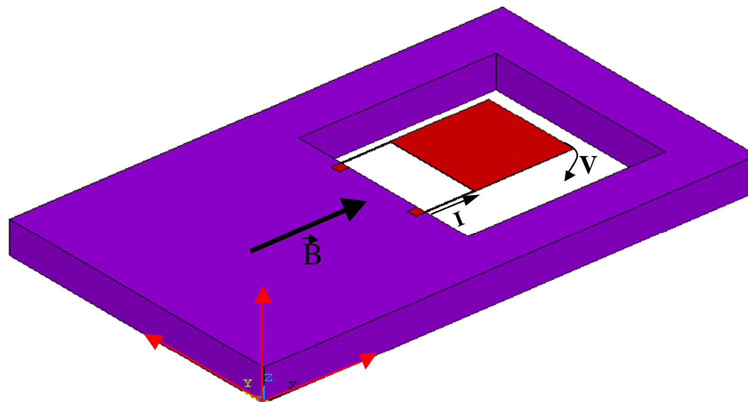

Figure 30. Cantilever used to detect a time-varying magnetic field.

To measure magnetic fields with cantilever structures, the Lorentz-force is utilized on a current carrying lead [50-52]. A cantilever of this type measures only the magnetic flux density in the direction parallel to the arms of the cantilever, i. e., x-axis of Fig. 30. The Lorentz-force acting on a lead is used to bend a micromachined cantilever. Deflections, which are small compared to the length of the cantilever, are a directly proportional measure of the applied force. To reach an as high as possible sensitivity it is advisable to utilize a resonant mechanism where the cantilever is excited by an AC current with a frequency equal to an eigenfrequency of the elastic structure. Due to the high quality factors of Si structures, which are at least several hundred, this is an efficient way to enhance the sensitivity.

Wafer Level Packaging

Fig. 31 shows how WLCSP can be used as an advantage to integrate the proposed antenna structure. It consists of three stacked wafers, where the bottom wafer is used to place the reading and controlling electronics, the middle wafer is used to implement the U-shaped

cantilever, and the bottom wafer encapsulates the device, enabling a very small microsystem with integrated antenna.

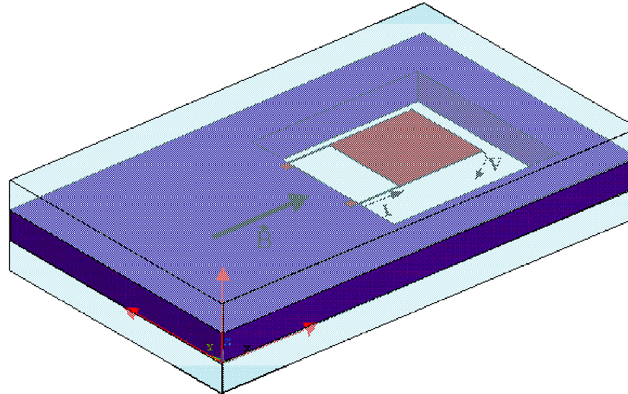

Figure 31. Use of WLCSP to integrate the proposed MEMS antenna.

Additionally, if it is added an energy-harvesting scheme, the microdevice is ready for use. If batteries are required, an extra step will be necessary to implement the required interface.

The starting MEMS structure is a cantilever placed to operate as a magnetic sensor, using the Lorentz force (see Fig. 30), where the electromagnetic field can be sensed using an optical, capacitive, or piezoelectric sensing solution. The most attractive options are capacitive and piezoelectric. These solutions can be easily integrated with the MEMS structure and have the potential for low power consumption (except the optical solution). Since the desirable displacement depends on structure dimensions and material properties, electrostatic actuation can be used as the actuation mechanism for MEMS micro-antennas. However, if large displacements are required or if the MEMS structure area becomes too small for capacitive detection, the use of a piezoelectric material can be the solution since it can act both as sensor and actuator. Moreover, the operation is only voltage based, leading to low power driving operation. Furthermore, it produces a voltage in response to a deflection leading to simple readout electronics.

Piezoelectric is a promising mechanism for realizing RF MEMS structures with low driving power and a wide continuous tuning range. A few papers have reported on piezoelectric actuators [48], which adopt ferroelectric PZT and a bulk MEMS process with wet etched holes through a Si DIE. PZT contains a high vapour pressure oxide of PbO, and requires repeated annealing at more than 600º C. These materials and processes make it difficult to be employed as a CMOS compatible process. To overcome those drawbacks, it was proposed piezoelectric actuator, which uses CMOS compatible AlN and Al as piezoelectric and electrode materials, and surface micromachining processes [49]. The deflection was proportional to the voltage and was in the range 0 – 10 um for a voltage range 0-5 V.

To radiate, the operation of the MEMS structure should be reversed and a field will be produced by an electrostatic or piezoelectric actuation.

Antenna Modelling

The research focus is now in MEMS structures for non-conventional front-ends, where the MEMS structure itself will be operating as an antenna. MEMS will be explored as a new solution to obtain structures that can sense and generate an electromagnetic field. Thus, instead of having the need to design very advanced antenna structures to achieve antenna size reduction, the standard MEMS devices, e.g. cantilevers, will be used to save system space and improve system integration.

The proposed MEMS structures will be engineered to have the desired electrical and geometrical properties, as well the requirements to be used in a post-process module compatible with integrated circuit (IC) fabrication.

Fig. 31 shows the model being used to analyse the receiving properties for a cantilever operating as an antenna.

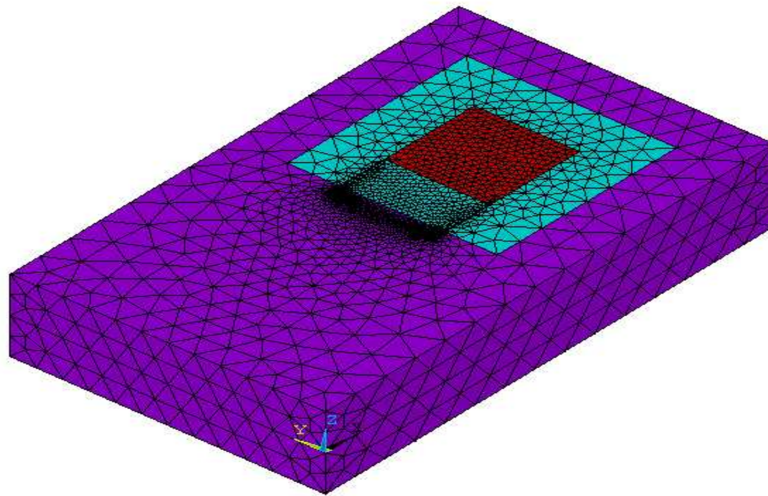

Figure 32. Model of structure used to sense the electromagnetic field.

The main goal is the design, fabrication and characterization of an electrically very small antenna using a MEMS structure. The main target will be implantable and invasive biomedical devices requiring low frequency wireless communications. However, the structures under research could also become a solution for underwater and underground communications. The research will allow to fully understand the bi-directional radiating properties and to optimise the radiation properties from an oscillating beam or cantilever. The driving properties of a piezoelectric material will be explored to obtain structures with large and bi-directional displacement. All the research will focus on low-power, low-size devices, as well the requirements to be used in a post-process module compatible with integrated circuit (IC) fabrication.

Antenna Results

To check the ability to operate as an antenna itself, some preliminary tests were conducted where it was verified that this MEMS structure could also have the potential to operate as a

bi-directional wireless link, together with the potential to be smaller than the conventional antennas.

To explore the possibility to use a magnetic sensor, it was used a scaled model of the proposed structure. A commercially available magnetic sensor was connected to a signal acquisition board that was connected to a personal computer. A current was injected into a scaled structure of Fig. 32 and the signal was recorded with the magnetic sensor. When the transmitting structure was oscillating at 100 KHz, it was possible to easily detect that signal with the magnetic sensor.

The received signal was compared with the signal received by a conventional dipole antenna and it was verified that the signal received by the magnetic sensor was easily detected. Thus, instead of having the need to design very advanced antenna structures to achieve antenna size reduction, the standard MEMS devices, e.g. cantilevers, can be used to save system space and improve system integration, when compared to the actual solutions.

Conclusion

This chapter described the design, fabrication and test of chip-size antennas for short-range wireless microsystems. These antennas allow the fabrication of a microsystem with integrated wireless communications. The antenna integration is based on wafer-level packaging techniques, which enables the integration of new materials with the standard silicon processing steps, as well the fabrication of complex three-dimensional structures. Wafer-level packaging techniques, like the adhesive wafer bonding and through-wafer vias, were used to overcome the challenge of obtaining a fully integrated microsystem, including the antenna, in an economically acceptable way.

The use of a folded patch was first explored as a solution for significant antenna area reduction, enabling the antenna integration with wafer-level packaging techniques and giving rise to a good spatial cover. The chip-size antenna works in the 5-6 GHz ISM band, with the small size making it well suited for low data-rate and short-range applications. Two types of antennas were fabricated: patch and folded patch. The patch antenna on glass (11,7x12,4 mm^2), operating at 5,995 GHz, has a gain of 3 dB, 100 MHz of bandwidth, and an efficiency of 51%. On the other hand, the patch antenna on silicon (8x8 mm^2), designed to operate at 5,705 GHz, has a gain of 0,3 dB, a bandwidth of 90 MHz and an efficiency of 19%. Finally, a folded patch antenna was designed on glass (4x4 mm^2) to operate at 5,1 GHz. It revealed a measured gain of approximately -8 dB, a bandwidth of ~200 MHz and a radiation efficiency of ~32%.

MEMS are then explored as a new solution to obtain structures that can sense and generate an electromagnetic field. Thus, instead of having the need to design very advanced antenna structures to achieve antenna size reduction, the standard MEMS devices, e.g. cantilevers, will be used to save system space and improve system integration.

The original contributions are: novel electrically very small antenna using MEMS structures, a model to describe the bi-directional operation of that structure; a radiating element that can be integrated on the same microsystem as the RF circuits, without affecting circuit requirements, and different material compositions in order to maximize the performance for the proposed applications.

References

[1] S. Remke, et al., "Wireless Capsule Endoscopy and Push-Enteroscopy in Chronic Gastrointestinal Bleeding: a Prospective Controlled Trial," *Gastrointestinal Endoscopy*, Vol. 55, No 5, 2002.

[2] J. T., Carlo, et al., "The Utility of Capsule Endoscopy and its Role for Diagnosing Pathology in the Gastrointestinal Tract," *The American Journal of Surgery*, Vol. 190, pp. 886-890, 2005.

[3] W.A. Qureshi, "Current and Future Applications of the Capsule Camera," *Nature Reviews*, Vol. 3, pp. 447-450, 2004.

[4] D. Fleischer, "Capsule Imaging," Clinical Gastrology and Hepatology, Vol. 3, 2005.

[5] P. Hunter Peckham, et al., "Functional Electrical Stimulation for Neuromuscular Applications," *Annu. Rev. Biomed*. Eng. 2005. 7:327–60, 35 pp., March 23, 2005.

[6] Muller N., "What Americans Understand How they Affected by Bladder Control Problems: Highlights of Recent Nationwide Consumer Research," Urologic Nursing. pp. 109-115, 2005.

[7] W. R Lenderking, JF Nackley, RB Anderson, MA Testa. "A review of the quality-of-life aspects of urinary urge incontinence; importance of patients' perspective and explanatory lifestyle," *J Am Geriatr Soc*., pp. 683-692, 1998.

[8] Robert A Gaunt, Arthur Prochazka, "Control of urinary bladder function with devices: successes and failures," *Progress in Brain Research*, Elsevier, Vol. 152, pp. 163-194, 2005.

[9] R. Macintosh, Lumbar Puncture and Spinal Analgesia, Blackwells Books, Oxford, 1951.

[10] Pedram Mohseni, et al., "Wireless Multichannel Biopotential Recording Using an Integrated FM Telemetry Circuit," *IEEE Trans. Neural. Syst. Rehab. Eng*., vol. 13, no. 3, pp. 263-270, Sept. 2005.

[11] P.M. Mendes, et al. "Integrated Chip-Size Antennas for Wireless Microsystems: Fabrication and Design Considerations," J. Sens. Act. A Physical, Vol. 125, No. 2, pp. 217-222, 10 Jan. 2006.

[12] Anders J. Johansson, "Wireless Communication with Medical Implants: Antennas and Propagation," PhD Thesis, Lund, Sweden , June 2004

[13] Ronald Kitchen, *RF Radiation Safety Handbook*, Butterworth-Heinemann, 1993.

[14] European Telecommunications Standards Institute, ETSI EN 301 839-1 Electromagnetic compatibility and Radio spectrum Matters (ERM);Radio equipment in the frequency range 402 MHz to 405 MHz for Ultra Low Power Active Medical Implants and Accessories;Part 1: Technical characteristics, including electromagnetic compatibility requirements, and test methods., 2002.

[15] Juan Hinojosa Jimenez, "Contribuition a l'Elaboration d'une Nouvelle Methode de Caracterisation Electromagnetique de Materiaux a Partir de Lignes Plaquees – Applications a l'Etude de Nouveaux Materiaux", Universite des Sciences et Technologie de Lille, Lille, France, These a Docteur de l'Universite, May 1995.

[16] P.M. Mendes, A. Polyakov, M. Bartek, J.N. Burghartz, J. H. Correia, "Extraction of Glass-Wafers Electrical Properties Based on S-Parameters Measurements of Coplanar Waveguides," ConfTele, June 2003, Portugal.

[17]Abdel-Hakim Boughriet, Christian Legrand, Alain Chapoton, “Noniterative Stable Transmission/Reflection Method for Low-Loss Material Complex Permittivity Determination”, IEEE Trans. Microwave Theory Tech., Vol. 45, nº 1, pp. 52-56, January 1997.

[18]Rainee N. Simons, *Coplanar Waveguide Circuits, Components and Systems*, John Wiley & Sons, 2001.

[19]Robert E. Collin, *Foundations for Microwave Engineering*, 2nd edition, McGraw-Hill, 1992.

[20]C. Veyres, V. F. Hanna, “Extension of the Application of conformal Mapping Techniques to Coplanar Lines with Finite Dimensions”, Int. J. Electron., Vol.48, nº. 1, Jan. 1980.

[21]William R. Eisenstadt, Yungseon Eo, “S-Parameter-Based IC Interconnect Transmission Line Characterization”, *IEEE Trans. Components*, Hybrids, and Manufact. Techn., Vol. 15, nº 4, pp. 483-489, August 1992.

[22]C. L. Holloway, E. F. Kuester, “A Quasi-Closed Form Expression for the Conductor Loss of CPW Lines, with an Investigation of Edge Shape Effects”, *IEEE Trans. Microwave Theory Tech.*, Vol. 43, nº 12, pp. 2695-2701, December 1995.

[23]Kin-Lu Wong, *Planar Antennas for Wireless Communications*, John Wiley & Sons, Inc., 2003.

[24]A. Polyakov, P.M. Mendes, S.M. Sinaga, M. Bartek, B. Rejaei, J.H. Correia, J.N. Burghartz, “Processability and Electrical Characteristics of Glass Substrates for RF Wafer-Level Chip-Scale Packages”, *in Proc. 53rd ECTC*, New Orleans, USA, 2003.

[25]P.M. Mendes, S. M. Sinaga, A. Polyakov, M. Bartek, J.N. Burghartz, J. H. Correia, “Wafer-Level Integration of On-Chip Antennas and RF Passives Using High-Resistivity Polysilicon Substrate Technology”, *In Proc. 54th ECTC,* Las Vegas, USA, 2004, pp. 1879 – 1884.

[26]P. M. Mendes, A. Polyakov, M. Bartek, J. N. Burghartz, J. H. Correia, “Integrated 5.7 GHz Chip-Size Antenna for Wireless Sensor Networks,” Transducers’03, Boston, USA, June 8-12, 2003, pp. 49-52.

[27]R.L. Li, G. DeJean, E. Tsai, E. Tentzeris, J. Laskar, “Novel small folded shorted-patch antennas”, *in Proc. Antennas and Propagation Soc. Int. Symp*., vol. 4, 2002, pp. 26-29.

[28]H. A. Wheeler, “Fundamental limitations of small antennas”, *Proc. IEE*, Vol. 35, pp 1479-1484, Dezembro 1947.

[29]L. J Chu, “Physical Limitations of Omnidirectional Antennas”, Technical report nº 64, *Research Laboratory of Electronics*, MIT, Maio 1948.

[30]R.F. Harrington, "Effect of Antenna Size on Gain, Bandwidth and Efficiency," Journal of research of national bureau of standards, D-radio Propagation, Vol. 64D, pp. 1-12, Janeiro 1960.

[31]R. E. Collin, S.Rothschild, “Evaluation of Antenna Q,” *IEEE Trans. Antennas Propagat*., Vol. AP-12, pp. 23-27, Janeiro 1964.

[32]R. L. Fante, “Quality Factor of General Ideal Antennas”, *IEEE Trans. Antennas Propagat*., Vol. AP-17, pp. 151-155, Março 1969.

[33]R. C. Hansen, “ Fundamental Limitations in Antennas”, *Proc. of the IEEE*, Vol. 69, pp. 170-182, Fevereiro 1981.

[34] J. S. McLean, "A Re-examination of the Fundamental Limits on the Radiation Q of Electrically Small Antennas", *IEEE Trans. Antennas Propagat.*, Vol. AP44, pp. 672-675, Maio 1996.

[35] R .L. Fante, "Maximum possible Gain for an Arbitrary Ideal Antenna with Specified Quality Factor", *IEEE Trans. Antennas Propagat.*, Vol. AP40, pp. 1586-1588, Dezembro 1992.

[36] J. C. Sten, A. Hujanem, "Notes on the Quality Factor an Bandwidth", *Springer-Verlag, Electrical Engineering*, Vol. 84, pp. 189-195, 2002.

[37] G. A. Thiele, Phil L. Detweiler, Robert P. Penno, "On the Lower Bound of the Radiation Q for Electrically Small Antennas," *IEEE Trans. Antennas Propagat.*, Vol. AP51, pp. 1263-1269, Junho 2003.

[38] G. S. Smith, "Efficiency of Electrically Small Antennas Combined with Matching Networks", *IEEE Trans. Antennas Propagat.*, Vol. AP25, pp. 369-373, Maio 1977.

[39] Wen Geyi, "Physical Limitations of Antenna," *IEEE Trans. Antennas Propagat.*, Vol. AP51, pp. 2116-2123, Agosto 2003.

[40] H. A. Wheeler, "Small Antennas", *IEEE Trans. Antennas Propagat.*, Vol. AP23, pp. 462-469, Julho 1975.

[41] D. Lange, O. Brand, and H. Baltes, *CMOS Cantilever Sensor Systems: Atomic Force Microscopy and Gas Sensing Applications*., Springer, 2002.

[42] J. S. Brooks, M. J. Naughton, Y. P. Ma, P. M. Chaikin, and R. V. Chamberlin, "Small sample magnetometers for simultaneous magnetic and resistive measurements at low temperatures and high magnetic fields," *Rev. Sci. Instr.*, **58**(1):117–121, 1987.

[43] M. J. Naughton, J. P. Ulmet, A. Narjis, S. Askenazy, M. V. Chaparala, and A. P. Hope, "Cantilever magnetometry in pulsed magnetic fields," *Rev. Sci. Instr.*, **68**(11):4061–4065, 1997.

[44] A. Agoston, F. Keplinger, and B. Jakoby, "A novel MEMS based viscosity sensor," In Proceedings of the Eurosensors 2004 - XVIII, pages B4.4 1–4, Rom, Italy, September 13–15 2004.

[45] T. Kabashima, et al., "A Study of the Cantilever Beam in Time Varying Magnetic Field," *IEEE Trans. on Magnetics*, Vol. 26, No. 2, pp. 563-566, March 1990.

[46] W. C. Tang, et al., "Laterally driven polysilicon microstructures," Sens. Actuators, vol. A20, pp. 25–32, 1990.

[47] L. A. Rocha, et al., "Analysis and analytical modeling of static pull-in with application to mems-based voltage reference and process monitoring," *J. Microelectromech. Syst.*, vol. 13, pp. 342–354, 2004.

[48] H.C. Lee, et al., "Piezoelectrically Actuated RF MEMS DC Contact Switches With Low Voltage Operation", IEEE Micro. Wirel. Comp. letters, Vol.15, No.**4**, pp.202-204, 2005.

[49] T. Kawakubo, et al., "Piezoelectric RF MEMS Tunable Capacitor with 3V Operation using CMOS Compatible Materials and Process," *IEEE IEDM Technical Digest*., pp. 294 – 297, 2005.

[50] V. Beroulle, Y. Bertrand, L. Latorre, and P. Nouet, "Monolithic piezoresistive CMOS magnetic field sensors," Sens. Actuators A, 103:23–32, 2003.

[51] F. Keplinger, S. Kvasnica, A. Jachimowicz, F. Kohl, J. Steurer, and H. Hauser, "Lorentz force based magnetic field sensor with optical readout," *Sens. Actuators A,* **110** (1–3):112–118, 2004.

[52] L. Latorre and P. Nouet, “A complete methodology for electro-mechanical characterization of a CMOS compatible MEMS technology,” *IEEE Trans. Electron.*, **E82-C**(4):582–588, 1999.